Photoelectrochemical and Optical Properties of Nitrogen Doped Titanium Dioxide Films Prepared by Reactive DC Magnetron Sputtering

Torbjörn Lindgren,[‡] Julius M. Mwabora,[‡,§] Esteban Avendaño,[‡] Jacob Jonsson,[‡] Anders Hoel,[‡] Claes-Göran Granqvist,[‡] and Sten-Eric Lindquist*[,†]

Department of Physical Chemistry, P.O. Box 579, and Department of Materials Science, P.O. Box 534, Uppsala University, SE−751 23 Uppsala, Sweden, and Department of Physics, University of Nairobi, P.O. Box 30197, Nairobi, Kenya

Received: October 30, 2002; In Final Form: January 28, 2003

Nanocrystalline porous nitrogen doped titanium dioxide (TiO_2) thin films were prepared by DC magnetron sputtering. Films were deposited in a plasma of argon, oxygen, and nitrogen, with varying nitrogen contents. The films were characterized by X-ray diffraction, scanning electron microscopy, and optical- and photoelectrochemical (PEC) measurements. These studies showed that the films were porous and displaying rough surfaces with sharp, protruding nodules having a crystal structure varying from rutile to anatase depending on the nitrogen content. All nitrogen doped films showed visible light absorption in the wavelength range from 400 to 535 nm. The PEC properties of the thin film electrodes were determined on as-deposited as well as dye-sensitized films. The nitrogen doped TiO_2 generated an incident photon-to-current efficiency response in good agreement with the optical spectra. The PEC measurements on dye-sensitized films showed that the electron-transfer properties in the conduction band were similar to those of undoped TiO_2. It was also experimentally confirmed that the states introduced by nitrogen lie close to the valence band edge. For the best nitrogen doped TiO_2 electrodes, the photoinduced current due to visible light and at moderate bias was increased around 200 times compared to the behavior of pure TiO_2 electrodes. There is an optimum in introduced nitrogen where the response is highest.

I. Introduction

Titanium dioxide, TiO_2, is a well studied and commonly used material for many photocatalytic[1] and photoelectrochemical[2] applications. In photocatalysis, it has been used for decomposition of water and degradation of organic pollutants in air as well as aqueous media. In photoelectrochemistry, it has been used in solar cell applications. TiO_2 combines good electrical properties with high catalytic activity and excellent stability in many solvents over a wide pH range. However, the band gap of the material, around 3.0 eV for rutile and 3.2 eV for anatase, allows only absorption of the ultraviolet, UV, part of the solar irradiation. Because this part of the solar spectrum only accounts for about 4% of the incoming solar energy, considerable efforts have been invested to broaden the photoresponse of the material so that also the less energetic but more abundant visible light is absorbed.

The normal way to achieve an enhanced absorption has been to attach various kinds of organic dyes to the surface. This approach has been successful for solar cell applications when combined with nanoporous TiO_2.[3] However, the commonly used ruthenium based dyes are expensive, and moreover, the long-term stability of many dyes can be questioned. Another obstacle with organic dyes is that they can detach from the surface when employed in aqueous solutions.

Also doping transition metals into TiO_2[4−6] and synthesis of reduced TiO_x[7,8] photocatalysts have been utilized for broadening the spectral response, but so far thermal instability and an increase of charge carrier recombination centers have limited the performance of the transition metal doped titanium oxide. [Doping is here used in a broad sense meaning modification of the material by foreign atoms. The amount of foreign atoms is considerably higher than traditionally used for doping for applications in electronics. Doping not only alters the charge-transfer properties but also affects the crystallinity and optical characteristics of the material.] Reduction of TiO_2 has been found to form states located 0.75 to 1.18 eV below the conduction band edge;[7] this lowers the photocatalytic driving force for reduction processes at the material since the photo-excited electrons will be of low energy. Also, the electron mobility in the bulk of the material will be reduced, because localized states are formed.

Recently, Taga et al.[9,10] successfully introduced a new approach to broaden the photoresponse of TiO_2 by doping with nitrogen. They reported that the optical absorption spectrum had a cutoff wavelength around 550 nm, which corresponded well with the threshold for photocatalytic activity. Another interesting oxy-nitride is $LaTiO_2N$ (with a band gap energy of 2.1 eV) introduced recently by Domen et al.,[11] who reported photo-activity under irradiation of visible light.

As shown in this present paper, we have taken the concept of nitrogen doping of TiO_2 further and introduced nitrogen in TiO_2 by means of reactive DC magnetron sputtering in a nitrogen containing plasma. The same sputtering setup was employed in an earlier work of ours to sputter deposited nanocrystalline "parallel penniform" TiO_2 with a large internal surface area.[12] To prepare the samples investigated below, we used deposition parameters similar to those described in ref 12

* To whom correspondence should be addressed. E-mail: sten@fki.uu.se.
† Department of Physical Chemistry, Uppsala University, Sweden.
‡ Department of Material Science, Uppsala University, Sweden.
§ Present and permanent address: Department of Physics, University of Nairobi, Kenya.

10.1021/jp027345j CCC: $25.00
Published on Web 05/24/2003

but with a current of 0.75 A and nitrogen also present in the sputter chamber during film fabrication.

In this first report on nitrogen doped thin films, we present photoelectrochemical as well as optical and crystal properties.

II. Experimental Section

Electrode and Electrolyte Preparation. Thin films were prepared according to a general thin-film sputtering method described by Rodriguez et al.[12] The same sputter parameters were used as in ref 13, though with a current of 0.75 A and an addition of nitrogen in the deposition chamber.

The nitrogen gas flow ratio, Φ, was kept constant during the deposition by mass-flow-controlled gas inlets; it is defined as

$$\Phi = f(N_2)/f \tag{1}$$

where f is the total flow rate, i.e.

$$f = f(O_2) + f(Ar) + f(N_2) \tag{2}$$

and $f(O_2)$, $f(Ar)$, and $f(N_2)$ are the individual flow rates of the gases. The $f(O_2)/f(Ar)$ gas flow ratio, Γ, was kept at a constant value of 0.06, whereas the total gas pressure was maintained at ~12 mTorr. Below we refer to Φ as the "nitrogen ratio".

For convenience, the films prepared with nitrogen will be called nitrogen doped TiO_2 and the films prepared without nitrogen will be called undoped TiO_2 (the authors are aware that also the latter films can be doped, for instance by oxygen vacancies).

The sputter deposited thin films were formed on soda lime glass substrates (standard microscope slides) for optical characterization and on electrically conductive glass for photoelectrochemical studies. The conducting glass substrates had a coating of fluorine-doped SnO_2 with a sheet resistance 8 Ω/□ (Tec8, Hartford Glass Company). Electrical contacts were established by fixing copper wires to the conducting layer on the glass substrate by use of conductive silver paint. Exposed areas of the back contact and edges were carefully sealed with epoxy resin. The working electrode area was about 0.5 cm^2 for each sample.

Sensitization of the films was made with a 5×10^{-4} M solution of cisdithiocyanato-bis(2,2′-bipyridyl-4,4′-dicarboxylate)-ruthenium (II) in ethanol, i.e., using a dye, known as N3,[14] that has shown good efficiency in earlier work. Prior to the sensitization, all films were kept in air at 450 °C for 5 min. They were then dipped into the dye solution while it was still warm (80 °C), and the films were kept immersed for 1 day.

Reagent grade chemicals and Milli-Q water (Millipore Corp.) were used for electrolyte preparations. The electrolytes selected in the present work were 0.1 M KI and 0.01 M K_2HPO_4/KH_2PO_4 buffers (pH 6.8) for three electrodes measurements and 0.5 M LiI and 0.05 M I_2 in ethylene carbonate/propylene carbonate (50:50 wt %) for two electrode measurements.

Characterization of Thin Films. The film thickness, determined by profilometry (Tencor Alpha Step), was around 850 ± 50 nm for all films. The nitrogen doped electrodes were bright yellow, transparent, and looked nonscattering to the eye. They were chemically, mechanically, and thermally stable under the experimental conditions used. As a test, a sample being a nitrogen-doped rutile TiO_2 film was annealed in an open atmosphere at 500 °C for 1 h without any change in the optical or photoelectrochemical properties. The microstructures of the films were analyzed by use of a LEO 1550 scanning electron microscope with a Gemini column, operating at 5 kV. Images were acquired using an inlens detector. The reflectance and transmittance data were measured using a specially designed absolute spectrophotometer.[15] The sample was measured at an angle of incidence of three degrees in both reflectance and transmittance. Because the absolute spectrophotometer is a specular instrument, we verified the recordings using a Perkin-Elmer Lambda 900 spectrophotometer fitted with a 150 mm integrating sphere. The two sets of measurements were in good agreement for the nitrogen doped samples, thus confirming that scattered light was not neglected in the absolute-recording instrument. The undoped sample showed some weak haze in the visible range; this effect was not taken into account for our analysis. The diffractometer was a Siemens D5000 instrument operating with Cu Kα radiation and equipped with a Göbel mirror in a conventional $\theta - 2\theta$ arrangement. The substrate employed for X-ray diffraction, XRD, was SnO_2:F coated glass. Data from standards[16] for TiO_2 were used to identify the diffraction peaks. The mean grain size, D, was determined from Scherrer's equation,[17] viz.

$$D = \frac{K\lambda_x}{\beta \cos \theta} \tag{3}$$

where K is a dimensionless constant, 2θ is the diffraction angle, λ_x is the wavelength of the X-ray radiation, and β is the full width at half-maximum of the diffraction peak.

The electrochemical cell used in the three-electrode experiments was a closed vessel with quartz windows and an inside wall of black Teflon to avoid reflection. Details of the experimental setup are given in ref 18. An Ag/AgCl electrode in saturated KCl (Metrohm AG) was used as a reference. According to the manufacturer's calibration, this reference electrode has a potential of +197 mV vs the normal hydrogen electrode, NHE, at 25 °C. The experiments were performed at 22 °C. The variation of the potential of the reference electrode at that temperature (compared to at 25 °C) was found negligible. All potentials mentioned in this study are referred to NHE. A platinum grid was used as a counter electrode in the cell. Both the reference and the counter electrode were enclosed in separate glass chambers with glass frits. For simulated solar irradiation, we used a Light Drive 1000 lamp (type 1400-E2/1, microwave powered sulfur plasma). The beam passed through an 80-mm-thick water filter to remove most of the infrared light. It was then passed through a timer-controlled shutter (Unibliz model VMM-T1) and then through a quartz glass into the electrolyte vessel. According to the specification for the lamp, the light intensity for wavelengths below 380 nm was less than 0.8% of the total output. The light intensity was measured by a pyranometer (Kipp & Zonen CM 11) and corrected through a calibration with direct sunlight. [The photoelectric conversion efficiency for a dye-sensitized TiO_2 nanostructured solar cell (usually called a Grätzel cell) was measured in direct sunlight at noon during a clear summer day in June. The current−voltage characteristic was then recorded by use of the Light Drive 1000 setup, and the position of the cell was adjusted to obtain the same $i-V$ curve as in the sun. The intensity of the lamp was then calibrated against the solar intensity. The reported values correspond to a solar intensity of 1000 Wm^{-2}.]

Current−voltage, $i-V$, measurements were performed at a light intensity of about 1000 Wm^{-2}. A computer-controlled potentiostat (Autolab μII, Eco Chemie BV) was used for all three-electrode photoelectrochemical experiments, both in darkness and under illumination. The electrolyte was mechanically

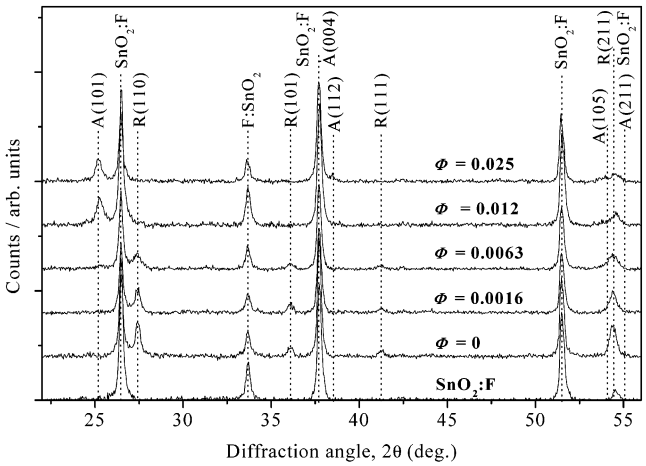

Figure 1. X-ray diffractograms for titanium dioxide films on SnO_2:F-coated glass substrates. At the bottom is the diffractogram of the pure substrate. The films were sputter deposited with five different nitrogen ratios, denoted Φ. The different peaks are assigned to different reflections in the anatase (A), rutile (R), and the substrate phases.

stirred and degassed by purging with nitrogen (99.99% purity) before and during each experiment. The voltage scan rate was 1 mV/s.

Our two-electrode experiments were carried out in a conventional sandwich-type cell, wherein the nitrogen doped TiO_2 electrode was clipped to a Pt foil counter electrode. The electrolyte was inserted into the cavity between the electrodes by capillary forces.

The experimental setup for incident photon-to-current efficiency, $IPCE_\lambda$, measurements was similar to the one shown in ref 19 but equipped with a Cermax model LX 300 UV lamp (ILC Technology) and a computer controlled 1/8m monochromator (CM 110) assisted by an automatic filter wheel (AB301, CM). The intensity was measured with an optical power meter (Newport, 1830-C). The light intensity was, typically, 1 mW/cm^2 at a wavelength, λ, of 470 nm. Specifically, the $IPCE_\lambda$ was calculated according to

$$IPCE_\lambda = \frac{hc}{e}\frac{I_{ph,\lambda}}{P_\lambda \lambda} \tag{4}$$

where $I_{ph,\lambda}$ is the photocurrent, P_λ is the power intensity of the light, and h, c, and e have their usual meanings of Planck's constant, speed of light in a vacuum, and elementary charge, respectively. $IPCE_\lambda$ plotted vs λ is called an "action spectrum". In all action spectra recorded with light incident onto the substrate electrode, SE, interface, corrections were made for absorption and reflection losses due to the conducting glass substrate. The transmission through the glass is less than 50% below 350 nm and the photocurrents are low, implying that this part of the corrected SE action spectra contained relatively large errors and are therefore not shown.

III. Results and Discussion

Crystal Structure of Sputtered Thin Films. Structural characterization of the Ti oxide films was performed by XRD. Figure 1 displays data for titanium dioxide films prepared with different, constant amounts of nitrogen in the sputter chamber. The XRD spectrum for the bare conductive substrate is shown in the lower part of Figure 1. The film prepared without nitrogen displays diffraction peaks from the underlayer, i.e., the conductive SnO_2 film, plus additional peaks belonging to rutile TiO_2. As the flow ratio of nitrogen during deposition, Φ, is increased, the rutile structure becomes less pronounced. With a gas mixture corresponding to Φ = 0.012 during deposition, an anatase structure starts to evolve. When the amount of nitrogen is increased further to Φ = 0.025, the anatase structure becomes more distinct. Scherrer's equation was applied to the anatase (101) and rutile (110) peaks and provided a mean grain size of around 20 nm for all films.

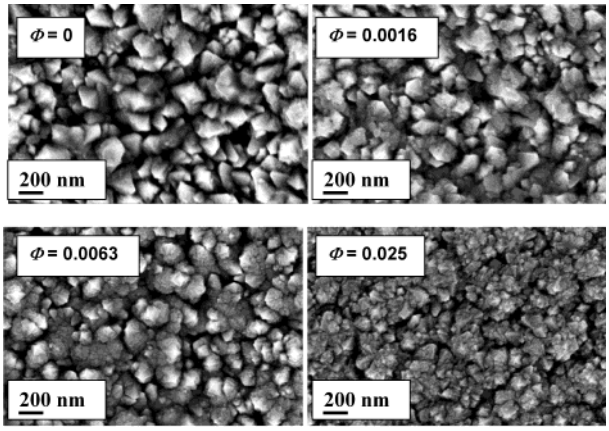

Figure 2. Scanning electron micrographs of titanium dioxide films sputter deposited with different nitrogen ratios, denoted Φ.

Surface Morphology of Sputtered Thin Films. Figure 2 shows scanning electron microscopy, SEM, images of the surfaces for four samples with different amounts of nitrogen used during deposition. Rough porous surfaces with sharp, protruding nodules are apparent in all films. The front surface of the TiO_2 film sputtered without nitrogen shows a three-dimensional porous network of interconnected titanium dioxide nodules, each being from 100 to 400 nm in size. The nodules become less pronounced when Φ is increased. A decrease in surface roughness by an increase of the nitrogen ratio during deposition was confirmed by atomic force microscopy. The standard deviation of the protrusion height decreased from about 60 nm for the undoped titanium dioxide to 30 nm for the film sputtered with Φ = 0.025. This decrease of the roughness is associated principally to the diminishing grain size.

The ratio between the electrochemically active area and the projected geometric area, ρ_{cv}, was obtained for undoped "parallel penniform" sputter deposited TiO_2 from cyclic voltammetry measurements by Gómez et al.[20] Their values of ρ_{cv} ranged from 600 for a 6.8-μm-thick film and a 150 for a 1.8-μm-thick film. Because our film preparation procedure is the same as that by Gómez et al., similar magnitudes are expected for our undoped electrodes. Adopting the values above for our undoped 0.85-μm-thick film, a ρ_{cv} of approximately 60 is expected. The SEM study indicated a more compact structure with increasing Φ values. Therefore, the roughness value mentioned above probably signifies an upper level for our electrodes.

Optical Properties of Sputter Deposited Thin Films. The absorption coefficient was determined by measuring reflectance, R, and transmittance, T, using optical spectrophotometry. Having these two quantities and the film thickness, d, the absorption coefficient, α, can be determined from the relation[21]

$$\alpha d = -\ln\left(\frac{T}{1-R}\right) \tag{5}$$

The model behind this formula applies when the refractive index of the substrate lies between 1.5 and 1.7 and the refractive index for the coating lies between 1.3 and 2.5. The approximation gives a relative error of around 10% and a maximum relative error less than 15% for higher refractive indices of the coatings.

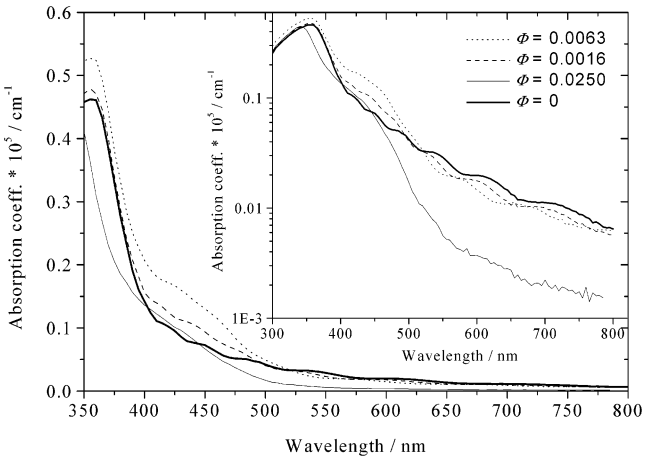

Figure 3. Spectral absorption coefficient for four films sputter deposited with different nitrogen ratios, denoted Φ. Absorption data are given on linear as well as logarithmic (inset) scales.

Our optical data, shown in Figure 3, correspond very well with the optical properties of nitrogen doped TiO_2 as reported by Taga et al.[10] The absorption is changed for the nitrogen-doped films so that it extends well into the visible light region and displays a threshold at a wavelength of 535 nm. It should be noted that the absorption coefficient does not rise as abruptly at 535 nm as it does for undoped TiO_2 at 410 nm. This suggests that the new spectral band, in the range $410 < \lambda < 535$ nm is not a band-to-band transition but rather is due to excitation of electrons from local states in the band gap to unoccupied states. Therefore, it is questionable if the term band gap narrowing, used by Taga et al.,[10] should be used to describe visible light absorption of nitrogen doped titanium oxide. The weak contribution to the absorption spectrum seen in the visible range for the undoped film is mainly caused by scattering.

The inset of Figure 3 illustrates a logarithmic dependence of the absorption coefficient on the wavelength. Clearly, there is a rather linear relationship between absorption coefficient and wavelength for $550 < \lambda < 800$ nm. This signifies a so-called Urbach tail,[22] which is related to fundamental properties of the material and not caused by thermal broadening. Many interpretations have been given to this tailing phenomenon, but no consensus has been reached as to its origins. Further discussion on the Urbach tail will be given elsewhere.[23]

Figure 4a shows the difference, on a logarithmic scale, of the absorption coefficient for the nitrogen doped films compared to the case of the undoped film (the formalism behind the calculation leading to Figure 4a is presented in ref 23). The shown results provide a rough estimation of the density of electronic states induced by the interaction between the 2p states of oxygen and the nitrogen orbitals, as described by Taga et al.[10] A quantitative analysis was difficult to accomplish for our data as a consequence of residual effects from interference fringes. The states seem to have a Gaussian distribution starting at an energy corresponding to 535 nm and peaking around 420−430 nm. Thus, we propose that the absorption band is due to a set of states centered around a maximum located approximately 2.9 eV below the lower edge of the conduction band. Further support for this assignment is given below. Taga et al.[10] identified the dominant transitions at the absorption edge with those from N $2p_\Pi$ to Ti d_{xy}', rather than transitions from O $2p_\Pi$ as in TiO_2.

Photoelectrochemical Studies of Sputtered Thin Films. $IPCE_\lambda$ was measured on as-deposited (i.e., pure nitrogen doped and undoped TiO_2) films as well as on dye-sensitized electrodes

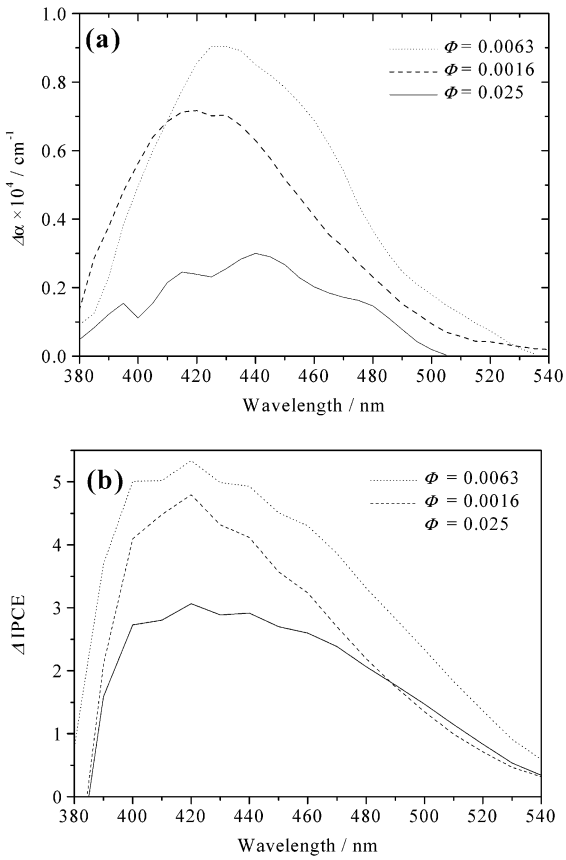

Figure 4. Part a shows the difference in absorption coefficient, α, between nitrogen-doped and undoped TiO_2. Part b illustrates the analogous difference in $IPCE_\lambda$ between nitrogen-doped and undoped TiO_2.

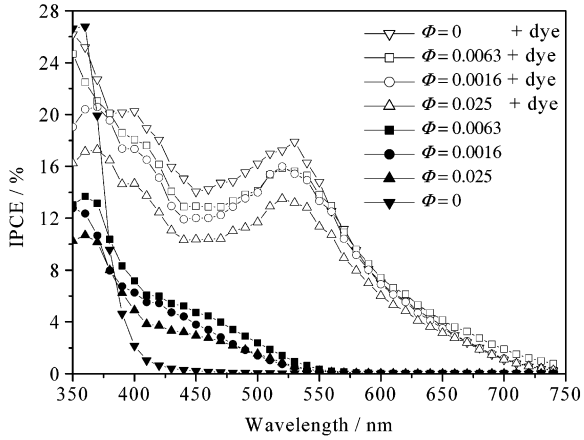

Figure 5. $IPCE_\lambda$ for as-deposited and dye-sensitized films of sputter deposited titanium dioxide in 0.5 M LiI and 0.5 mM I_2 in ethylene carbonate/propylene carbonate (50:50 wt %) studied in a two-electrode setup. No bias was applied, and the illumination was from the substrate/electrolyte interface.

based on these films. Undoped sputter deposited TiO_2 ($\Phi = 0$) was used as a reference sample. The photoelectrochemical response of the nitrogen doped TiO_2 was studied for pure rutile ($\Phi = 0.0016$) films, for pure anatase films ($\Phi = 0.025$), and for films having a mixture of anatase and rutile crystal structure ($\Phi = 0.0063$) vide infra.

Two-Electrode Measurements of $IPCE_\lambda$ for As-Deposited Films. Figure 5 shows spectral action spectra for films prepared with different nitrogen flow ratios in the sputter chamber during deposition. Data for the as-deposited TiO_2 films correspond well

with the optical properties of the films presented in Figure 3. For undoped TiO_2, the onset of photoresponse starts at a wavelength around 410 nm and extends into the UV region. This is typical for rutile titanium dioxide, characterized by a band gap of around 3.0 eV. The onset of the photoelectrochemical response of the nitrogen-doped samples is located around 540 nm, which is again consistent with the optical data.

It is interesting to relate the observed differences in absorption coefficient between the nitrogen doped and undoped films, $\Delta\alpha$, in the range $380 < \lambda < 540$ nm (Figure 4a) with the $IPCE_\lambda$ differences between the nitrogen doped and undoped films, $\Delta IPCE_\lambda$, in the same wavelength interval (Figure 4b). It can be seen that the spectral distribution of $\Delta IPCE_\lambda$ resembles the distribution of $\Delta\alpha$ for all three films. This suggests that it is mainly the optical characteristics which determine the unbiased photoelectrochemical response of the new band in the visible region. To some extent, small variations in crystal structure between the samples can also affect the observed difference. Therefore, we would not expect a complete overlap of the absorption spectra and action spectra in Figure 4, parts a and b. So far, we have no explanation to the empirical fact that the optical absorption of the new band in the visible wavelength range goes through an optimum for a mass flow rate ratio around $\Phi = 0.0063$.

Using an average film thickness of 850 nn and the maximum values of $\Delta\alpha$ and $\Delta IPCE_\lambda$ in Figure 4, parts a and b, we can estimate the so-called absorbed photon to current efficiency, $\Delta APCE_\lambda$. Applied to data in Figure 4, the simple relation is $\Delta APCE_\lambda = \Delta IPCE_\lambda/(1 - T)$, where $1 - T$ is a measure of the absorption. One can easily estimate T from the absorbance, A, through the relation $A = \Delta\alpha d = -\lg T$. The estimated values of $\Delta APCE_\lambda$, obtained from the three curves corresponding to Φ being 0.0063, 0.0016, and 0.025 in Figure 4 are 6.4, 6.3, and 6.8%, respectively. This means that only six to seven electrons per a hundred absorbed photons will contribute to the current in the outer circuit. The question is then in what processes is more then 90% of the generated charge carrier is lost? This will be discussed in further detail below.

Returning to Figure 5, we also observe that in the UV region the nitrogen doped TiO_2 electrodes show lower $IPCE_\lambda$ values than in the undoped film. This is a typical photoelectrochemical behavior for films with states in the band gap. These states can act as recombination centers for light induced charge carriers, which lower the photoresponse, as here observed in the UV region. For solar energy applications, this loss will be negligible because the solar energy in the UV region is small compared to that in the visible region. In the work by Taga et al.,[10] the photocatalysis observed under visible light was attributed to active sites of substitutional N identified with the atomic β-N states by XPS measurements combined with theoretical analyses. Their XPS measurements indeed showed the additional β-N states peaking at 396 eV.

Two-Electrode Measurements of $IPCE_\lambda$ for Dye-Sensitized Films. Electron transfer across the semiconductor solution interface plays a vital role with regard to solar energy conversion in a dye-sensitized photoelectrochemical solar cell, DSC.[2] In these cells, a dye adsorbed at the semiconductor surface absorbs light with an energy less than the semiconductor band gap energy. The excited dye molecule then injects an electron into the conduction band of the semiconductor. This electron injection has been found to be remarkably fast,[24] thereby facilitating a fast charge separation of the light induced charge carriers and contributing to high solar energy conversion efficiencies. Recently, Schnadt et al.[25] reported that the time needed to inject an electron from a dye molecule into a semiconductor was in the sub-3-fs regime. At the moment of injection, a positive charge, i.e., a hole, is created on the dye, which in a regenerative DSC is captured by an electron donor in the electrolyte. In our cell, this is I^-. It is important to note that no holes are formed in the valence band of the semiconductor during the absorption. Therefore, electron−hole recombination in the semiconductor is not possible, unless the hole on the dye molecule is transferred to the semiconductor. This is an improbable process in the case of the $(N3)^+$ dye molecular ion on a bare titanium dioxide ($\Phi = 0$) film electrode, because the upper edge of the valence band is well below the energy level of the highest occupied molecular (HOMO) level of the $(N3)^+$.

For the DC magnetron sputtered TiO_2 films, dye sensitized with N3, there is no major difference between the action spectra of the films no matter what nitrogen flow rate ratio was used (in the range $0 < \Phi < 0.025$) during deposition (see Figure 5). Now if we assume, in accordance with Taga et al.,[10] that the states introduced by nitrogen doping of the TiO_2 are in a range above the upper edge of the TiO_2 valence band but below the HOMO level of $(N3)^+$, we can explain the observed similarities between the spectra of the dye-sensitized films in Figure 5. The slight dissimilarities between the dye-sensitized films in this figure, we believe, are caused by somewhat different porosities among the samples, which gives a variation in the dye content of the films. The small difference between the electrodes can also be due to minor variations in film thickness and crystal structure. Nevertheless, the overall similarity of the intensity of the $IPCE_\lambda$ spectra in Figure 5 for the N3 dye sensitized TiO_2 films suggests that nitrogen doped TiO_2 films are able to handle the electron transport in the conduction band equally well as the undoped TiO_2 films.

Returning to the photoresponse of the nitrogen doped unsensitized TiO_2 electrodes, as given by the action spectra in Figures 4b and 5, we propose that the relatively low $APCE_\lambda$ values (6 to 7%, as calculated above) of these films in the visible region ($400 < \lambda < 540$ nm) are due to a poor hole transport in the semiconductor and/or a slow hole transfer at the semiconductor−electrolyte interface.[19] The nitrogen induced states in the band gap, close to the valence band in the bulk and/or at the electrode surface, adds to this because they can work as traps for holes promoting recombination of the light induced charge carriers. Because the same electrolyte is used for the nitrogen doped and the undoped TiO_2, we propose that the main reason for recombinations in the nitrogen doped TiO_2 are related to problems of transferring the holes to the semiconductor−electrolyte interface. In other words, the transport of holes in the nitrogen-induced band gap states is not as good as the hole transport in the valence band of undoped titanium dioxide. We therefore suggest that the hole transport in the nitrogen doped TiO_2 is the limiting factor for the photoelectrochemical response of the as-deposited nitrogen doped TiO_2. A more detailed study of the origin of the recombinations in nitrogen doped TiO_2 is in preparation.[26]

Position of the Nitrogen Band Gap States. Because the electron transport in the conduction band of the nitrogen doped and undoped TiO_2 is similar, and the $APCE_\lambda$ of these films were low, we proposed above that the states introduced by nitrogen rather are located close to the valence band edge than close to the conduction band edge. It is not obvious that this should be the case, though. For instance, in the III−V semiconductor GaInAs, nitrogen has been used to decrease the band gap,[27] and

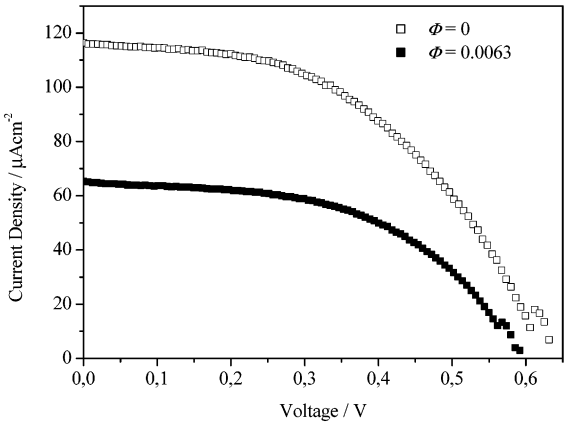

Figure 6. *i*−*V* characteristics for solar cells based on titanium dioxide films sputter deposited with different nitrogen ratios, denoted Φ.

in that case, the position of the conduction band is altered by the presence of nitrogen.

To further ensure that the position of the conduction band edge is not changed by the presence of nitrogen (apart from the difference of 0.2 eV between the conduction band edges of rutile and anatase), the open circuit potential of the dye-sensitized sandwich cell mentioned above was illuminated with white light from a sulfur plasma solar simulator, and the open circuit potential was measured. The open circuit potential is defined as the difference between the quasi-Fermi potential of electrons in the semiconductor and the redox potential in the electrolyte. Because the quasi-Fermi potential of electrons in an *n*-doped semiconductor lies close to the conduction band edge, a lowering of the conduction band edge would decrease the open circuit potential. From Figure 6, it is evident that the conduction band edge remains unchanged by nitrogen doping, because the open circuit potential is almost the same with and without nitrogen doping of the dye-sensitized cell. This experimental result is again in agreement with the calculations by Taga et al.,[10] who showed, by the highly precise full-potential linearized augmented plane wave formalism,[28] that the nitrogen-created states are located from the valence band edge and upward into the band gap of TiO_2.

Three-Electrode Measurements *i*−*V* Characteristics. Figure 7 illustrates the performance of the sputtered thin film titanium dioxide electrodes in a three-electrode setup under white light illumination. The *i*−*V* curves were swept toward negative potentials at a scan rate of 1 mVs^{-1}. The light from the sulfur plasma lamp, described in the Experimental Section, was chopped on and off at intervals of 15 s. The electrolyte was a 0.1 M KI, pH = 6.8 aqueous solution. As can be seen in Figure 7, the white light from the lamp hardly causes any photoresponse for the undoped film electrode (Figure 7a), whereas the photocurrent is enhanced for the nitrogen doped TiO_2 electrodes (Figure 7, parts b and d). Comparing the samples made at Φ = 0.0063 and 0 at anodic potentials, the photocurrent of the former is up to 200 times larger. However, the nitrogen-doped material is suffering from considerable electron−hole recombination. This is apparent from the pronounced photocurrent transient observed in a broad range around the onset potential, U_{on}, of photocurrent at about −0.1 V; the approximate position of U_{on} is indicated by a circle in Figure 7c. These transients, as well as the more or less linear increase of the photocurrent above 0.3 V, are signs of a high electron−hole recombination rate in the nitrogen-doped electrode materials.

Despite the substantial losses due to recombination, the nitrogen-doped material has an improved photoresponse in visible light, compared to the case of undoped TiO_2. This makes the nitrogen-doped material an interesting candidate for photocatalytic applications in liquid as well as in gas-phase systems.

As can be seen in Figure 7, the most pronounced increase in photoresponse of the film electrodes is achieved at a nitrogen flow ratio of 0.0063. In agreement with the action spectra given in Figures 5 and 4b, there is an optimum somewhere around Φ = 0.0063 for best performance of the nitrogen-doped films. Further optimizations of the deposition conditions, as well as

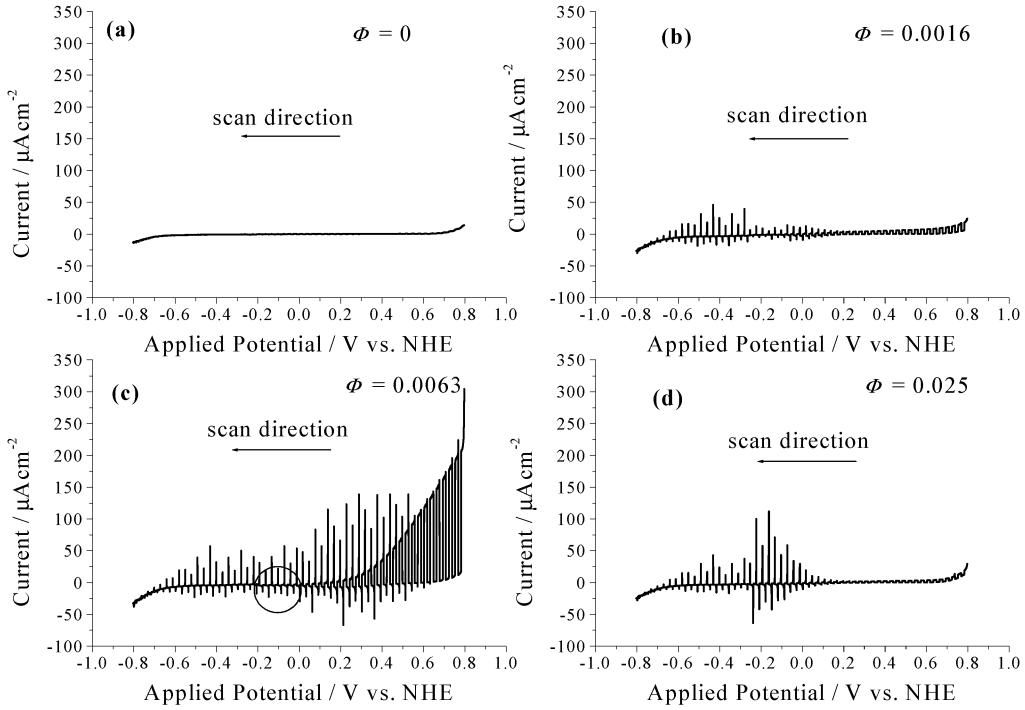

Figure 7. *i*−*V* characteristics of titanium dioxide electrodes sputter deposited with different nitrogen ratios, denoted Φ. The electrodes were mounted in a three-electrode setup and illuminated from the substrate/electrolyte interface in a 0.1 M, pH = 6.8 aqueous electrolyte.

an optimization of the film thickness, should lead to even more efficient electrodes.

The difference in photoresponse for the various nitrogen doped films is mainly due to the difference in the amount of absorbed visible light, as already shown in Figure 4, but it could to some extent also be ascribed to the small variation in film thickness, the variation in morphology, and the fact that the film electrodes have different crystal structures (see Figure 1). The latter may be a relatively important factor. It should be noted in this context that the effective mass of the electrons, and accordingly their mobility, varies between rutile and anatase.[29] This affects the charge transport in the electrode material and thus also the photoresponse as it, with increasing incorporation of nitrogen the crystal structure, changes from rutile to anatase (Figure 1). Although the best performance is obtained for films with a rutile, Φ was approaching the value where anatase films were obtained. Gomez[30] earlier observed the best performance for a mixture of rutile and anatase for "parallel penniform" TiO_2. A crystal mixture is also expected for our films prepared at $\Phi = 0.0063$ with the mixture mainly consisting of rutile as seen in the XRD measurements.

As mentioned above, the potential U_{on} for photocurrent at pH 6.8 for the film electrode made at $\Phi = 0.0063$ (Figure 7c) is located at around -0.1 V vs NHE. Ideally, the onset potential of the anodic photocurrents should coincide with the flatband potential, U_{fb}.[31] However, in reality, extensive recombinations lead to an anodic shift of the onset potential from the flat band potential. Adopting the flat band potential at pH = 0, i.e., $U_{fb} = -0.16$ V vs NHE, for nanostructured anatase as given in the literature,[32] and accepting a Nernstian behavior with pH, we would expect an onset potential at -0.56 V vs NHE for the nitrogen-doped TiO_2 at pH = 6.8. This is far from the observed value, being -0.1 V. The undoped TiO_2 showed an onset located around -0.4 V at pH = 6.8. A more extended study on the effect of pH and recombinations on the onset potential for sputtered TiO_2 will be presented elsewhere.[26] We interpret this difference in onset potential of a (readable) photocurrent as a consequence of the electron−hole recombination in the bulk and/or at the surface of the electrode. A shift in U_{on} due to a downshift of the energy position of conduction band edge caused by the nitrogen doping cannot immediately be neglected. However, with the result of the two-electrode measurements in mind (Figure 6), we are inclined to favor the strong electron−hole recombination as the major reason for the anodic shift of U_{on}.

Three-Electrode Measurements of IPCE$_\lambda$ for As-Deposited Films. The IPCE$_\lambda$ for the film electrode made at $\Phi = 0.0062$ was also studied in a three-electrode setup; see Figure 8. The electrolyte was aqueous 0.1 M KI, pH = 6.8, and the applied potential was 0.6 V vs NHE. The dark current was negligible.

It can be seen in Figure 8 that the photoresponse is higher for illumination in the SE direction for both nitrogen-doped and undoped TiO_2. This is a typical behavior of a nanoporous film[33] wherein the charge carriers, produced in the vicinity of the back contact, are collected more efficiently. For the undoped TiO_2, the photoresponse was similar for backside and front-side illumination, which indicates that the nanoporous film has a far from optimal film thickness. A thicker film would no doubt give a more pronounced difference. Currently, we are fabricating thicker films for optimum performance of the sputter deposited nanoporous nitrogen-doped electrodes.

IV. Summary

Nanoporous nitrogen-doped TiO_2 films were successfully prepared by reactive DC magnetron sputtering. XRD showed that the crystal structure was sensitive to the gas mixture in the sputter plasma. By increasing the amount of nitrogen used in the chamber during deposition, the crystal structure could be changed from rutile to anatase. SEM studies showed that all films had rough surfaces with protruding nodules. The surface roughness decreased with the amount of nitrogen used, as was also indicated by AFM. All samples prepared with nitrogen showed an optical response in the 400 to 535 nm wavelength range. The high uptake of dyes, when soaking the films in an N3 dye solution, clearly demonstrated that the films were porous and had a large inner surface area. Front-side and backside action spectra further supported that the films were porous.

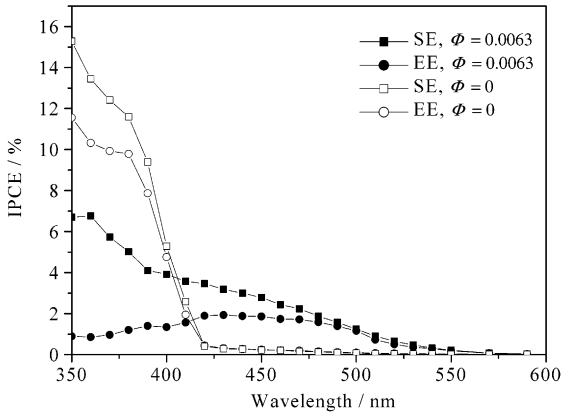

Figure 8. *IPCE*$_\lambda$ for as-deposited titanium dioxide electrodes sputter deposited with different nitrogen ratios, denoted Φ, in a 0.1 M KI, pH = 6.8 aqueous electrolyte. The electrodes were mounted in a three-electrode setup and biased to 0.6 V vs NHE. Irradiation took place from the substrate side and from the electrolyte side, denoted SE and EE, respectively.

Action spectra for as-deposited films were in good agreement with the corresponding optical spectra. The *IPCE*$_\lambda$ was also studied for the dye-sensitized films. The analysis of those spectra strongly indicated that the electron transport in the conduction band of nitrogen doped TiO_2 is, in the main, the same as in undoped TiO_2. Therefore, it was proposed that hole transports in the semiconductor and at the electrode/electrolyte interface were limiting factors for the photoelectrochemical performance of the nitrogen-doped electrodes. Consistent with the latter, it was also suggested that nitrogen-induced states in the band gap and/or at the electrode surface are acting as recombination centers for the light induced charge carriers. White light measurements of the open circuit potential of dye-sensitized nitrogen-doped films could be understood on the premise that the position of the conduction band edge remains unchanged by nitrogen doping.

Despite the intense recombination caused by the nitrogen doping, the new band gap states created by the doping indeed improve the photoresponse for white light at the expense of some losses of UVresponse. The photocurrent in white light of nitrogen-doped TiO_2 film electrodes increased by about a factor 200 (at anodic potentials) compared to the case of an undoped TiO_2 film electrode. There is an optimum in introduced nitrogen where the response is highest.

The proven industrial viability of magnetron sputtering, and our ability to control the sputtering parameters to achieve a variety of nitrogen doped nanostructured TiO_2 films of suitable film thickness, makes further work to optimize the performance of the nitrogen-doped TiO_2 of considerable interest for future photocatalytic applications. Such work is currently in progress.

Acknowledgment. The Swedish National Energy Administration has supported this work. We thank M. Sc. Magnus W.

Larsson at the Department of Materials Chemistry, Lund Institute of Technology, for help with the AFM. Dr. H. Rensmo at the Department of Physics at Uppsala University is acknowledged for valuable discussions. J.M.M. thanks the International Science Program at Uppsala University for a fellowship. E.A. is grateful for the scholarship received from the University of Costa Rica to complete the PhD program at Uppsala University.

References and Notes

(1) Fujishima, A.; Hashimoto, K.; Watanabe, T. *TiO_2 Photocatalysis*; Bkc, Inc.: Tokyo, Japan, 1999.
(2) Hagfeldt, A.; Grätzel, M. *Acc. Chem. Res.* **2000**, *33*, 269.
(3) O'Regan, B.; Grätzel, M. *Nature* **1991**, *353*, 737.
(4) Sakata, Y.; Yamamoto, T.; Okazaki, T.; Imamura, H.; Tsuchiya, S. *Chem. Lett.* **1998**, *12*, 1253.
(5) Sakata, Y.; Yamamoto, T.; Gunji, H.; Imamura, H.; Tsuchiya, S. *Chem. Lett.* **1998**, *2*, 131.
(6) Iwasaki, M.; Hara, M.; Kawada, H.; Tada, H.; Ito, S. *J. Colloid Interface Sci.* **2000**, *224*, 202−204.
(7) Cronemeyer, D. C. *Phys. Rev.* **1959**, *113*, 1222.
(8) Breckenridge, R. G.; Hosler, W. R. *Phys. Rev.* **1953**, *91*, 793.
(9) Morikawa, T.; Asahi, R.; Ohwaki, T.; Aoki, K.; Taga, Y. *Jpn. J. Appl. Phys.* **2001**, *40*, L561.
(10) Asahi, R.; Morikawa, T.; Ohwaki, T.; Aoki, K.; Taga, Y. *Science* **2001**, *293*, 269.
(11) Kasahara, A.; Nukumizu, K.; Hitoki, G.; Takata, T.; Kondo, J. N.; Hara, M.; Kobayashi, H.; Domen, K. *J. Phys. Chem. A* **2002**, *106*, 6750.
(12) Rodríguez, J.; Gómez, M.; Lu, J.; Olsson, E.; Granqvist, C. G. *Adv. Mater.* **2000**, *12*, 341.
(13) Gómez, M.; Rodríguez, J.; Lindquist, S.-E.; Granqvist, C. G. *Thin Solid Films* **1999**, *342*, 148.
(14) Hagfeldt, A.; Grätzel, M. *Chem. Rev.* **1995**, *95*, 49.
(15) Nostell, P.; Roos, A.; Rönnow, D. *Rev. Sci. Instr.* **1999**, *70*, 2481.
(16) 2001 JCPDS (Int. Center for Diffraction Data); files 87-0920 and 86-1157
(17) Cullity, B. D. *Elements of X-ray Diffraction*; Addison-Wesley: Reading, MA, 1959.
(18) Lindgren, T.; Wang, H.; Beermann, N.; Vayssieres, L.; Hagfeldt, A.; Lindquist, S.-E. *Sol. Energy Mater. Sol. Cells* **2002**, *71*, 231.
(19) Rensmo, H.; Lindström, H.; Södergren, S.; Willstedt, A.-K.; Solbrand, A.; Hagfeldt, A.; Lindquist, S.-E. *J. Electrochem. Soc.* **1996**, *143*, 3173.
(20) Gómez, M.; Rodríguez, J.; Tingry, S.; Hagfeldt, A.; Lindquist, S.-E.; Granqvist, C. G. *Sol. Energy Mater. Sol. Cells* **1999**, *59*, 277.
(21) Hong, W. Q. *J. Phys. D: Appl. Phys.* **1989**, *22*, 1384.
(22) Urbach, F. *Phys. Rev.* **1953**, *92*, 1324.
(23) Mwabora, J. M.; Lindgren, T.; Avendaño, E.; Lindquist, S.-E.; Niklasson, G.; Granqvist, C.-G. Paper in preparation.
(24) Benkö, G.; Kallioinen, J.; Korppi-Tommola, J. E. I.; Yartsev, A. P.; Sundström, V. *J. Am. Chem. Soc.* **2002**, *124*, 489.
(25) Schnadt, J.; Brühwiler, P. A.; Patthey, L.; O'Shea, J. N.; Södergren, S.; Odelius, M.; Ahuja, R.; Karis, O.; Bässler, M.; Persson, P.; Siegbahn, H.; Lunell, S.; Mårtensson, N. *Nature* **2002**, *418*, 620.
(26) Romualdo Torres, G.; Lindgren, T.; Granqvist, C.-G.; Lindquist, S.-E. Paper in preparation.
(27) Shan, W.; Walukiewicz, W.; Ager, J. W., III.; Haller, E. E.; Geisz, J. F.; Friedman, D. J.; Olson, J. M.; Kurtz, S. R. *Phys. Rev. Lett.* **1999**, *82*, 1221.
(28) Wimmer, E.; Krakauer, H.; Weinert, M.; Freeman, A. J. *Phys. Rev. B* **1981**, *24*, 864.
(29) Asahi, R.; Taga, Y.; Mannstadt, W.; Freeman, A. J. *Phys. Rev. B* **2000**, *61*, 7459.
(30) Gómez, M. Ph.D. Thesis, Universidad Nacional de Ingeniería, Lima, Peru, 2001.
(31) Lindquist, S.-E.; Vidarsson, H. *J. Mol. Catal.* **1986**, *38*, 131.
(32) Rothenberger, G.; Fitzmaurice, D.; Grätzel, M. *J. Phys. Chem.* **1992**, *96*, 5983.
(33) Hagfeldt, A.; Björkstén, U.; Lindquist, S.-E. *Sol. Energy Mater. Sol. Cells* **1992**, *27*, 293.